Res Chem Intermed (2017) 43:2103–2118
DOI 10.1007/s11164-016-2749-7

Synthesis of mesoporous Ca-MCM catalysts and their use in suitable multicomponent synthesis of polyfunctionalized pyrans

Eliana Nope[1] · José J. Martínez[2] · Hugo A. Rojas[2] · Ángel G. Sathicq[1] · Gustavo P. Romanelli[1,3]

Received: 27 June 2016 / Accepted: 30 September 2016 / Published online: 7 October 2016

Abstract Mesoporous Ca-MCM catalysts were prepared using a mixture of $CaCO_3$, TEOS, cetyl trimethyl ammonium bromide (CTAB), triethanolamine (TEA), ethanol and H_2O. Three catalysts with different $CaCO_3$ contents, M-Ca 1 %, M-Ca 5 % and M-Ca 10 %, respectively, were prepared and characterized by N_2 physisorption, XRD, FT-IR, XPS, TPD-CO_2 and Pyridine-FTIR. A green and simple protocol was developed for the synthesis of 6-amino-4*H*-pyran scaffolds through a multicomponent coupling reaction of an aldehyde, malononitrile, and 1,3-dicarbonyl compound in different reaction solvents. This procedure was performed at room temperature (20 °C), obtaining good and excellent yields of 4*H*-pyran derivatives. The mesoporous materials are insoluble in polar media, which allows easy removal of the reaction products without affecting their catalytic activity. The leaching test showed an excellent stability, and Ca-MCM catalysts can be used three times without appreciable loss of their catalytic activity.

Keywords Mesoporous Ca-MCM · Polyfunctionalized 4*H* pyrans · Multicomponent reaction

✉ José J. Martínez
jose.martinez@uptc.edu.co

✉ Gustavo P. Romanelli
gpr@quimica.unlp.edu.ar

[1] Centro de Investigación y Desarrollo en Ciencias Aplicadas 'Dr. Jorge J. Ronco' (CINDECA-CCT-CONICET), Universidad Nacional de La Plata, Calle 47 No. 257, B1900AJK La Plata, Argentina

[2] Escuela de Ciencias Químicas, Facultad de Ciencias, Universidad Pedagógica y Tecnológica de Colombia UPTC, Avenida Central del Norte, Tunja, Boyacá, Colombia

[3] Cátedra de Química Orgánica, CISAV, Facultad de Ciencias Agrarias y Forestales, Universidad Nacional de La Plata, La Plata, Argentina

Introduction

Heterogeneous catalysis plays an important role in the production of chemical products. The use of heterogeneous catalysis has several benefits; for example, it can be separated easily by simple filtration, which is a relevant topic for industrial manufacturing processes due to economical and environmental considerations. The development of inexpensive, mild, reusable, nontoxic catalysts tolerating a wide range of temperatures, and easy and safe disposal remains an issue of great interest [1–3].

The need for clean processes imposes the use of different environmentally friendly reaction conditions such as a procedure at room temperature, the elimination of toxic solvent, transformation with high atom economy and the use of a recyclable catalyst [4]. In particular, ethanol is considered a green solvent, because it poses few human health and environmental risks, and ethanol is mostly derived from the fermentation of biomass feedstocks [5].

Another aspect that contributes to achieving a cleaner process is the substitution of inorganic or organic liquid catalysts, such as aqueous sodium and potassium hydroxide or sodium methoxide or terbutoxide, for a reusable solid basic catalyst Recently, different materials, such as metal oxides, rare earth oxides, modified hydrotalcites, clays, natural phosphates, anion exchanger resin, and the alkylammonium group on MCM-41, have been used to catalyze different transformations, under mild reaction conditions, with high selectivity, easy recovery, catalyst recycling, and simple product isolation [6, 7]. In this direction, Tanabe and Hölderich reviewed the industrial applications of solid acid and base catalysts. They counted more than 100 industrial processes in which solid acid, base, and acid–base bifunctional catalysts are used [8].

Recently, mesoporous molecular sieves (such as MCM-41, MCM-48, and SBA-15) have attracted much attention in catalysis due to the specific characteristics of these materials that include high surface area, well-defined pore shape, narrow pore size distribution, and good thermal stability [9].

These materials are very attractive for heterogeneous reactions of large organic molecules for which microporous zeolites cannot be used. Kubota et al. obtained excellent results in the Knoevenagel condensation using Si-MCM-41 molecular sieves. Recently, Pirouzmand and coworkers prepared Ca/MCM-41 via direct and post-synthesis methods, and they studied the effect of the cationic template and metal incorporation method on their basicity and catalytic performance in the transesterification reaction of canola oil [10, 11].

On the other hand, multicomponent reactions (MCRs) are a notable methodology in heterocyclic synthesis for obtaining molecular diversity. MCRs increase the reaction efficiency due to their high atom economy, which involves performing several steps without isolating intermediates or changing the reaction conditions. MCRs have attracted attention in the area of combinatorial chemistry due to their efficiency [12, 13].

Furthermore, heterocyclic compounds bearing the 4*H*-pyran skeleton are an important family of compounds that play a key role in organic synthesis, because they are present in a variety of synthetic compounds. Synthetic molecules

containing the pyran moiety have interesting pharmacological and biological properties [14]. These compounds are used as anticancer, spasmolytic, anticoagulant, anti-anaphylactic, neuroprotective, HIV-inhibitory, antimicrobial, antifungal, antioxidant agents, and some have diuretic activity [15]. 4*H*-Pyrans containing a heterocyclic ring are extensively used in pharmacology; for example, 4-phenyl-4*H*-pyrans have been identified as potent and specific IK_{Ca} channel blockers, and some 2-amino-4*H*-pyrans are important photoactive materials [16].

The most common synthesis of 2-amino-4-aryl-3-cyano-4*H*-pyran derivatives is usually a two-step reaction carried out between a Michael acceptor (arylidene-malononitriles) and β-dicarbonyl compounds in the presence of a base as catalyst (piperidine, morpholine or metal alkoxides) using ethanol or other solvents (DMSO, DMF) as reaction media. Most of these methods involve volatile solvents that require longer reaction times and the catalyst is difficult to recover [17].

To solve these disadvantages, methods that involve recyclable solid basic catalysts have been reported. For example, $FeNi_3$–SiO_2 [18], potassium phthalimide (POPI) [19], nanosilica-supported tin (II) chloride [12], imine-based silica-functionalized copper(II) [20], nanocrystalline ZnO [15], sodium acetate [21] copper II oxymetasilicate [22], silica nanoparticles [17], sodium borate [23], ZnO/MgO [24], ammonium acetate [25], and Mg/La mixed oxide [26] afforded excellent yields of 4H pyrans.

In the present paper, we report the synthesis and characterization of three mesoporous solids containing $CaCO_3$. In addition, we studied the application of these recyclable solid catalysts in a simple, convenient, efficient, and eco-friendly process for the multicomponent preparation of 2-amino-4-aryl-3-cyano-4*H*-pyran derivatives (Fig. 1). To the best of our knowledge, this is the first application of this type of solids in multicomponent reactions using a green and simple protocol at room temperature for the synthesis of 6-amino-4*H*-pyran scaffolds.

Experimental section

General

The precursors and additives tetraethyl orthosilicate (TEOS), $CaCO_3$, cetyl trimethylammonium bromide (CTAB), ethanol (EtOH), NH_4OH, and tri-ethanolamine (TEA) were used in the catalyst preparation. Aromatic aldehydes

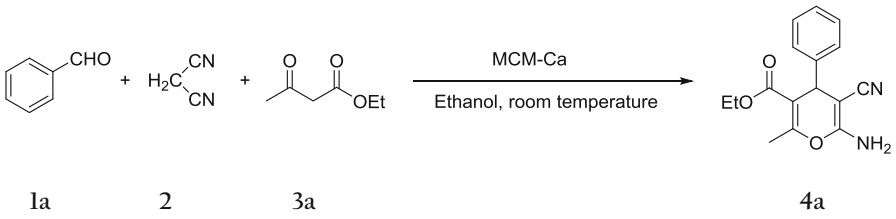

Fig. 1 Synthesis of 6-amino 4*H*-pyran derivative via a three-component coupling of benzaldehyde **1a**, malononitrile **2** and ethylacetoacetate **3a**

such as malononitrile and 1,3-diketo compound were used in the synthesis of 4*H*-pyrans. All chemicals were purchased from Aldrich and used without further purification.

Benzylidene malononitrile was prepared following the procedure described in the literature [27]. The reaction yields were calculated from pure products. All the products were identified by comparison of melting point (mp), thin layer chromatography (TLC), and nuclear magnetic resonance (NMR) data. ^{1}H and ^{13}C NMR spectra were recorded on a Bruker (400 MHz) spectrometer using TMS as internal reference. Chemical shifts for ^{1}H NMR and ^{13}C NMR spectra were reported using ($CDCl_3$) as solvent. ^{13}C NMR spectra were recorded at 100 MHz.

Catalyst syntheses

Ca-MCM solids (M-Ca 1 %, M-Ca 5 % and M-Ca 10 %) were prepared at different concentrations of $CaCO_3$ using ethanol as co-solvent at room temperature. The molar composition of the gels was: 1 SiO_2: X $CaCO_3$: 0.3 CTAB: 170 H_2O: 74.8 EtOH: 4.7 NH_4OH: 0.2 TEA. Where, X was the % $CaCO_3$ incorporated (1, 5, and 10 %, respectively). CTAB and TEA were used as template agents. In a typical procedure, a solution of CTAB and NH_4OH and $CaCO_3$ was mixed carefully in ethanol for 60 min. Then, a solution of TEOS and TEA was added dropwise and stirred for 24 h. The pH was 10.5. The gels were dried at room temperature and then calcined in air flow ($10\ cm^3 \times min^{-1}$) at 550 °C. Si-MCM was synthetized following the same procedure.

Catalyst characterization

Textural properties

N_2-sorption isotherms at 77 K were measured in Micromeritics ASAP 2020 equipment. Samples were previously evacuated at 623 K for 16 h. The surface area was calculated using a multipoint Brunauer–Emmett–Teller (BET) model in the range of $P/P^0 = 0.05 - 0.35$ in the adsorption isotherm. The pore volume was calculated from the amount of N_2 adsorbed at the highest relative pressure of 0.99, and the pore diameter was calculated from the Barrett–Joyner–Halenda (BJH) equation.

X-ray diffraction

X-ray diffraction studies were performed in a PANalytical X-Pert-Pro diffractometer using nickel filtered Cu kα radiation ($\lambda = 1.54056$ Å). Spectra were obtained in the range 1.5°–4° and 10°–100° using a count time of 1 s and a step size of 0.05°. The unit cell parameter (Å) was calculated using the formula $a = \sqrt{6}d$, where d represents the d (211) reflection.

Fourier transform infrared spectroscopy

The FTIR spectra were recorded on KBr pellets on a Perkin–Elmer FTIR 2000 spectrometer.

XPS analysis

The XPS data were obtained in a Thermo Scientific Escalab 250 XI spectrometer. Measurements were performed at room temperature with monochromatic Al Kα ($h\nu = 1486.6$ eV) radiation. The analyzer was operated at 25 eV pass energy and a step size 0.05 eV. The pressure in the analytical chamber was 6.3×10^{-9} mBar. The C 1 s signal (284.6 eV) was used as internal energy reference in every experiment. The determination of core-level peak positions was accomplished after background subtraction according to Shirley using peak XPS software. Peaks in a spectrum were fitted by a combination of Gauss and Lorentz curves, which also allowed the separation of overlapping peaks.

Temperature-programmed desorption of CO_2 (TPD-CO_2)

The nature of basic sites was studied by temperature-programmed desorption of CO_2. TPD analysis was performed on a Micromeritics AutoChem 2920. Prior to the adsorption of CO_2, the samples were preheated at 300 °C in He flow (25 mL/min) for 1 h. Then, the adsorption of CO_2 (10 % in helium) at 50 mL/min was carried out at 120 °C for 30 min. The samples were purged with helium (25 mL/min) for 1 h. The TPD began at 90 °C K with a heating rate of 10 °C/min to reach 900 °C.

Pyridine adsorption followed by FTIR

The nature of acid sites was studied by pyridine (Pyr) adsorption, followed by FTIR. Infrared spectra were collected using Nicolet iS50 equipment with an in situ diffuse reflectance cell (Harrick, Praying Mantis). For the determination of acid sites, a pretreatment at 573 K was performed with a helium flow of 30 mL/min for 1 h to clean the surface of possible contaminants. Subsequently, the samples were gradually cooled down to room temperature and then pyridine adsorption was performed for 1 h to 10 mL/min. After adsorption, the gas phase was removed by evacuation with a helium flow at 30 mL/min at 573 K.

General procedure for the synthesis of 4H-pyranes

The catalytic activity of the CaO-MCM catalysts was evaluated in the formation of 4*H*-pyranes. The reaction was performed in a round bottom flask equipped with a condenser and immersed in an oil bath. Briefly, a mixture of aldehyde (1 mmol), malononitrile (1 mmol), 1,3-diketo compound (1 mmol), and the catalysts (30 mg) was stirred at room temperature (20 °C) in 2 mL ethanol. The progress of the reaction was monitored by TLC (EtOAc/hexane = 1:1). After completion of the reaction, 2 mL of ethanol was added to the reaction mixture to remove the catalyst.

Upon concentration of the reaction mixture, the desired product crystallized out. The crude product was recrystallized from ethanol to give a pure product. As the purity of the product was high, no further recrystallization was required.

Catalyst reuse

Reuse stability tests of the catalysts were carried out by running five consecutive experiments, under the same reaction conditions. After each test, the catalyst was separated from the reaction mixture by filtration, washed with ethanol (2 × 2 mL), dried under vacuum, and then reused.

H-NMR and ^{13}C-NMR spectra of selected pyranes

*Ethyl 6-amino-5-cyano-2-methyl-4-phenyl-4H-pyran-3-carboxylate (**1**)* ^{1}H NMR (400 MHz, $CDCl_3$): δ 1.15 (t, 3H, $J = 7.2$ Hz), 2.41 (s, 3H), 4.00 (m, 2H, $J = 7.2$ Hz), 4.40 (s, 1H), 4.63 (s, 2H), 7.22–7.37 (m, 5H); ^{13}C NMR (100 MHz, $CDCl_3$): δ 13.8, 18.5, 38.4, 60.2, 62.3, 108.2, 118.9, 127.3, 127.7, 128.4, 143.6, 156.5, 156.6, 157.5, 165.3

*Ethyl 6-amino-5-cyano-2-methyl-4-p-tolyl-4H-pyran-3-carboxylate (**2**)* ^{1}H NMR (400 MHz, $CDCl_3$): δ 1.09 (t, 3H, $J = 7.2$ Hz), 2.30 (s, 3H), 2.38 (s, 3H), 4.06 (q, 2H, $J = 7.2$ Hz), 4.39 (s, 1H), 4.54 (s, 2H), 7.10 (m, 4H); ^{13}C NMR (100 MHz, $CDCl_3$): δ 13.7, 18.3, 21.4, 38.2, 60.9, 62.2, 108.2, 119.1, 127.2, 129.1, 136.7, 140.9, 156.5, 157.3, 166.2

*Ethyl 6-amino-5-cyano-2-methyl-4-(3-nitrophenyl)-4H-pyran-3-carboxylate (**4**)* ^{1}H NMR (400 MHz, $CDCl_3$): δ 1.12 (3H, t, $J = 7.2$ Hz), 2.40 (3H, s), 4.00–4.06 (2H, m), 4.55 (1H, s), 4.85 (2H, s), 7.46–7.52 (2H, m), 8.03–8.08 (2H, m); ^{13}C NMR (100 MHz, $CDCl_3$): δ 14.2, 18.8, 39.1, 61.1, 107.1, 118.6, 122.5, 122.6, 129.7, 134.1, 146.3, 148.5, 158.1, 165.5

*Ethyl 6-amino-5-cyano-4-(3-hydroxyphenyl)-2-methyl-4H-pyran-3-carboxylate (**5**)* ^{1}HNMR (400 MHz, $CDCl_3$), δ 1.00 (t, 3H, $J = 7.2$ Hz), 2.37 (s, 3H), 4.05 (q, 2H, $J = 7.2$ Hz), 4.34 (s, 1H), 4.72 (s, 2H), 6.63–6.69 (m, 3H), 7.10 (t, 1H), 8.80 (s, 1H); ^{13}CNMR (100 MHz, $CDCl_3$), δ 13.8, 15.4, 38.8, 58.2, 61.0, 107.1, 112.2, 114.9, 117.4, 121.7, 124.1, 129.8, 143.4, 155.8, 159.1, 167.2

*Ethyl 6-amino-5-cyano-2-methyl-4-(3,4,5-trimethoxyphenyl)-4H-pyran-3-carboxylate (**8**)* ^{1}H NMR (400 MHz, $CDCl_3$), δ 1.12 (t, 3H, $J = 7.2$ Hz), 2.45 (s, 3H), 3.82 (s, 9H), 4.10 (q, 2H, $J = 7.2$ Hz), 4.43 (s, 1H), 4.68 (s, 2H), 6.53 (s, 2H); ^{13}C NMR (100 MHz, $CDCl_3$), δ 13.8, 18.8, 56.0, 60.6, 62.4, 104.3, 107.7, 137.1, 139.4, 153.3, 156.1, 157.2, 165.9

*Methyl 6-amino-5-cyano-2-methyl-4-phenyl-4H-pyran-3-carboxylate (**10**)* ^{1}H NMR (400 MHz, $CDCl_3$), δ 2.30 (s, 3H), 4.00 (s, 3H), 4.40 (s, 1H), 4.50 (s, 2H),

7.15–7.28 (m, 5H); ^{13}C NMR (100 MHz, $CDCl_3$), δ 18.0, 38.4, 51.9, 62.0, 107.5, 118.7, 127.2, 127.4, 128.4, 143.5, 157.0, 157.4, 166.5

*Methyl 6-amino-4-(2-chlorophenyl)-5-cyano-2-methyl-4H-pyran-3-carboxylate (**12**)* ^{1}H NMR (400 MHz, $CDCl_3$), δ 2.30 (s, 3H), 3.60 (s, 3H), 4.53 (s, 1H), 5.00 (s, 2H), 7.08–7.30 (m, 4H); ^{13}C NMR (100 MHz, $CDCl_3$), δ 18.0, 36.5, 51.2, 61.1, 106.8, 118.0, 127.3, 128.4, 128.8, 129.8, 133.1, 140.5, 157.7, 157.8, 166.2

Results and discussion

The nitrogen sorption isotherms are shown in Fig. 2. The isotherms are of type IV in the IUPAC classification. In all samples, the capillary condensation step occurs at a relative pressure of $\sim$0.2. The absence of a hysteresis loop in this region indicates a high quality mesoporous framework in the Ca-MCM solids. The pore size distributions calculated according to the Barrett, Joyner and Halenda method (BJH-method) suggest a very narrow pore size distribution in Si-MCM and Ca-MCM, which is centered between 2.2 and 2.7 nm depending on the $CaCO_3$ content. This slight change in pore size is possibly due to the presence of calcium carbonate inside the channels.

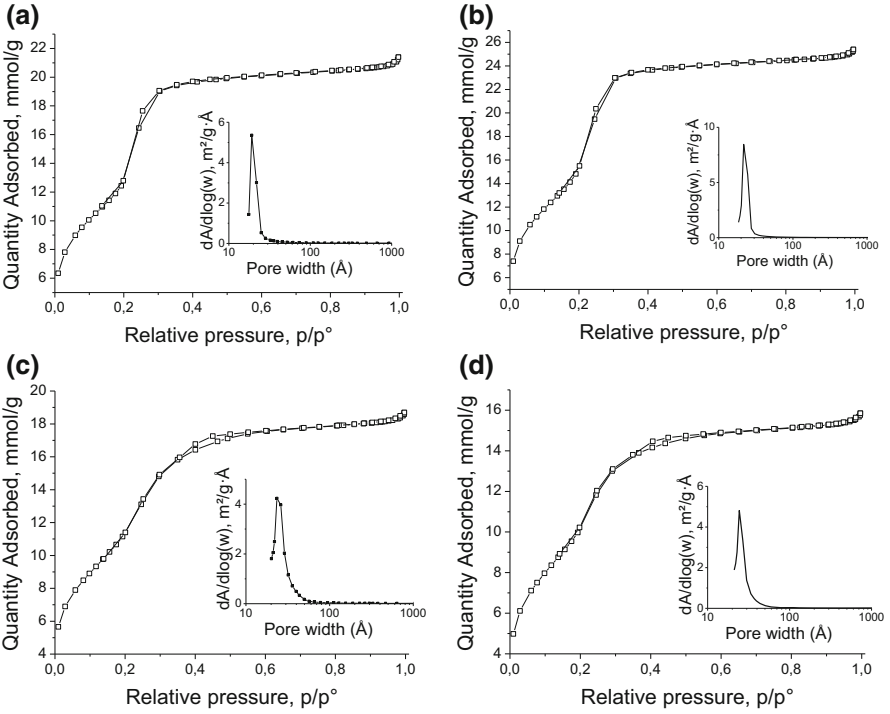

Fig. 2 Nitrogen sorption isotherms of the calcined Ca-MCM solids. **a** Si-MCM, **b** Ca-MCM 1 %, **c** Ca-MCM 5 %, **d** Ca-MCM 10 %

The textural properties of all prepared solids are summarized in Table 1. In general, the solids have high surface areas (961–1590 $m^2\ g^{-1}$) and pore volumes between 0.54 and 0.9 $cm^3\ g^{-1}$. The thickness of the silica pore walls can be easily calculated using the reflection angle obtained for each sample and the pore diameter. The values are between 1.1 and 1.3 nm, indicating the good quality of the mesoporous structure. However, the thickness of Ca-MCM is less compared with that of Si-MCM. It is well recognized that the pore wall thickness is related to longer crystallization times; however, the poor solubility of $CaCO_3$ allows that not all the $CaCO_3$ is included inside the pores of mesoporous solid, and there is not incorporation of Ca into MCM framework resulting in a lower thickness of Ca-MCM compared with Si-MCM. It is possible that in our solids Ca-MCM have some clusters of $CaCO_3$; however, the activity catalytic shown is similarly independent of $CaCO_3$ content, and this being the most interesting result in this study.

The X-ray diffraction patterns at low angle range (1.5°–4°, Fig. 3a) of calcined Ca-MCM are shown in Fig. 1a. A peak at $2\theta \sim 2.4°$ to 2.7° in all samples can be observed (Table 1). The incorporation of $CaCO_3$ slightly modifies the interplanar distance in the mesoporous solid sample due to the presence of $CaCO_3$ particles inside the channels. The XRD pattern at wide angle (Fig. 3b) shows a well-defined diffraction peak and a broad peak at 22° associated with SiO_2. Other peaks perfectly match the standard calcite pattern (JCPDS 88-1807, red line). The peaks increase with the calcite contents in the mesoporous structure. The crystal size of $CaCO_3$ using the (1 0 4) reflection peak at $2\theta = 29.36°$ is near 3.0 nm. This size is similar in every catalyst (Fig. 3).

The incorporation of $CaCO_3$ was also followed by FTIR (Fig. 4). In the region of 1050–1100 cm^{-1} a band assigned to Si–O bond vibration appears [28]. The displacement at higher wave number of this band is attributed to the interaction Ca–O–Si, which is more evident with increasing calcite content. This phenomenon also, has been observed in Ca-SBA [29].

Figure 5 shows the XPS spectra of the Ca 2p core levels for all Ca-MCM catalysts. The $Ca2p_{3/2}$ core level binding energy (BE) position appears at 346 eV, which is characteristic of a calcite structure. This result confirms that the calcination temperature for preparing the Ca-MCM solids does not modify the $CaCO_3$ structure.

CO_2-TPD studies were used to compare the basicity of Ca-MCM solids. Figure 6 depicts the temperature-programmed desorption spectra of two representative Ca-MCM catalysts (1 and 5 %). The peak observed at around 600 °C could be assigned to the thermal decomposition of $CaCO_3$, so only CO_2 desorption is observed in the range of 100–400 °C (inset in Fig. 5). The desorption of CO_2 at 150 °C showed the existence of –OH groups associated with weak basic sites, while the signal at around 280 °C corresponds to moderate strength basicity. The signal at 150 °C is well defined in the Ca-MCM 5 % catalyst (Fig. 4b). According to the integral intensity of the desorption curves, the total basicity of the Ca-MCM catalysts increases with the calcite content.

The FTIR spectra of pyridine adsorbed on the surface of MCM and Ca-MCM are shown in Fig. 7. The solid $CaCO_3$-MCM present both Lewis and Brönsted acid sites related with the mesoporous framework. The Lewis acid sites (L) on the surface can be recognized with the bands at 1444 and 1577 cm^{-1} [30]. This band decreases with

Table 1 Textural and crystallographic properties of the calcined Ca-MCM solids

Mesoporous material	Surface area (m^2/g) BET	Surface area (m^2/g) *t* plot	Pore volume (cm^3/g)	Pore diameter (nm)	Pos. [°2Th.]	d_{211} spacing (Å)	$a_0 = 2/\sqrt{3}$ d_{211} (Å)	Wall thickness (nm) = a pore diameter
MCM	1332	1142	0.74	2.2	2.63	33.5	38.7	1.7
Ca-MCM 1 %	1587	1580	0.88	2.4	2.91	30.3	34.9	1.1
Ca-MCM5 %	1057	1113	0.63	2.7	2.70	32.7	37.8	1.1
Ca-MCM 10 %	961	1187	0.54	2.4	2.76	31.9	36.9	1.3

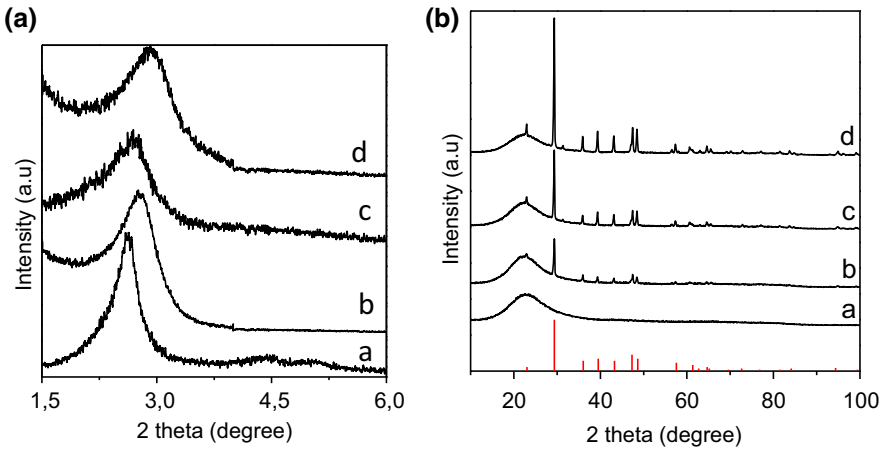

Fig. 3 X-ray diffraction patterns at (**a**) low-angle range and (**b**) high-angle range of the calcined Ca-MCM: *a* Si-MCM, *b* Ca-MCM 1 %, *c* Ca-MCM 5 %, *d* Ca-MCM 10 %

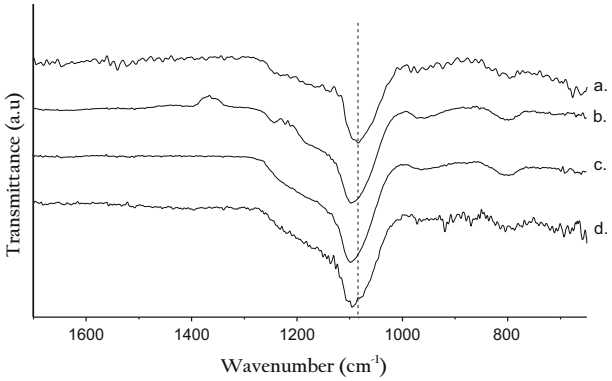

Fig. 4 FTIR spectra for *a* Si-MCM, *b* Ca-MCM 1 %, *c* Ca-MCM 5 %, *d* Ca-MCM 10 %

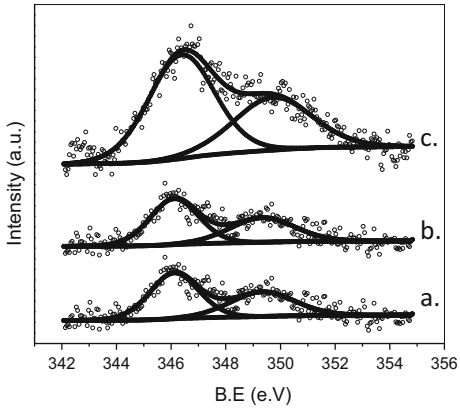

Fig. 5 XPS spectra of the Ca 2p core levels of the calcined Ca-MCM. *a* Ca-MCM 1 %, *b* Ca-MCM 5 %, *c* Ca-MCM 10 %

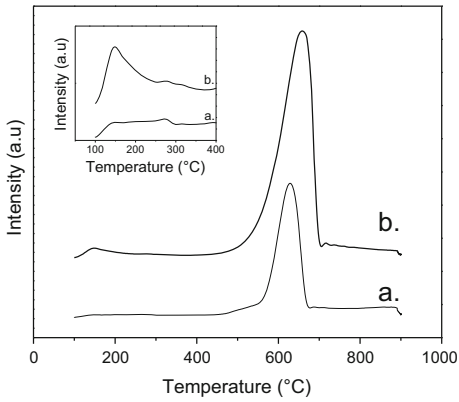

Fig. 6 CO_2 desorption patterns for *a* Ca-MCM 1 % and *b* Ca-MCM 5 %

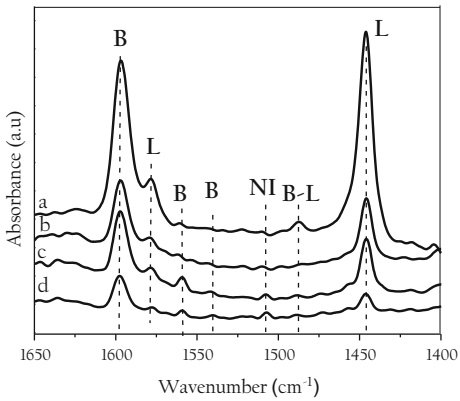

Fig. 7 FTIR spectra of pyridine adsorbed for *a* MCM, *b* Ca-MCM 1 %, *c* Ca-MCM 5 % and *d* Ca-MCM 10 %

the presence of $CaCO_3$. The bands at 1540 and 1596 cm^{-1} in MCM are associated with Brönsted acid sites (B). The band at 1540 cm^{-1} is attributed to formation of the pyridinium ion, and the signal at 1596 cm^{-1} corresponds to Brönsted acid sites, which are not strong enough to protonate pyridine, but these sites could form hydrogen bonded adducts [31]. It is interesting to note that these bands decrease in Ca-MCM solids, but a new band at 1560 cm^{-1} appears also, and this has been associated with Brönsted acid sites [32]. The signal in 1490 cm^{-1} is characteristic of Lewis–Brönsted acid sites (B–L) [29].

Catalytic test

Initially, we focused on the evaluation of different catalysts for the model reaction between benzaldehyde (**1a**), malononitrile (**2**) and ethylacetoacetate (**3a**) in ethanol at room temperature. We used Ca-MCM 1, 5 and 10 % to improve the yield for the synthesis of 2-amino-4*H*-pyran compounds. The reaction without catalyst (Table 2, entry 1) gives only the product of condensation between benzaldehyde and malononitrile. When commercial bulk $CaCO_3$ is used, a yield of 4*H*-pyran is

Table 2 Optimization of reaction conditions using different synthetized catalysts

	Yield intermediate I	Yield 4*H*-pyran	Ca content
Blank	95	0	0
$CaCO_3$	5	90	100
Ca-MCM 1 %	7	98	0.9
Ca-MCM 5 %	6	86	4.2
Ca-MCM 10 %	7	86	8.6

Reaction conditions Benzaldehyde (1 mmol), malononitrile (1 mmol), and ethyl acetoacetate (1 mmol) were stirred in 2 mL of ethanol in the presence of 30 mg of M-Ca 1 % at room temperature (20 °C) for 12 h

obtained (Table 2, entry 2), indicating that the presence of a catalyst is necessary to improve the reaction. As shown in Table 2, a most interesting result is obtained with MCM-Ca 1 %. In this case, the yield to 4*H*-pyran is 84 % at room temperature (20 °C) in 12 h, and the calcium content is very low, only 0.9 % (Table 2, entry 3). Finally, the yields for 4*H*-pyran using Ca-MCM 5 and 10 % catalysts are similar and independent of the load of $CaCO_3$ (Table 2, entries 4 and 5). This indicates that less than 1 % of calcium is sufficient to perform the reaction with excellent yields and selectivity.

Then, we performed the reaction in various solvents in order to optimize the reaction conditions using Ca-MCM 1 % as catalyst (Table 3). The results confirmed that the solvent has a great effect on the catalytic activity of Ca-MCM. The reaction was favored by the presence of polar solvents such as ethanol, methanol or water (Table 3, entries 1–3), and the yields were very low when we used less polar solvents such as toluene or chloroform, 38 and 45 %, respectively (Table 3, entries 5 and 6). The highest yield was obtained with ethanol, 98 % (Table 3, entry 1).

The reuse of the catalyst was evaluated under the same reaction conditions and proportions (1 mmol each substrate, 2 mL of ethanol, 30 mg of Ca-MCM 1 %, 20 °C, 12 h) in five consecutive cycles of reaction. The separation is by simple filtration due to the hydrophobicity of the Ca-MCM solid in comparison with

Table 3 Solvent screening for the model reaction

Entry	Solvent	Yields (%)
1	Ethanol	98
2	Methanol	91
3	Water	85
4	Acetone	45
5	Toluene	38
6	Chloroform	35

Reaction conditions Benzaldehyde (1 mmol), malononitrile (1 mmol), and ethyl acetoacetate (1 mmol) were stirred in 2 mL of ethanol in the presence of 30 mg of M-Ca 1 % at room temperature (20 °C) for 12 h

Table 4 Catalyst reuse, effect on 4*H*-pyran (%)

Entry	Catalytic cycle	Yield (%)
1	1	98
2	2	95
3	3	95
4	4	94
5	5	93

Reaction conditions Benzaldehyde (1 mmol), malononitrile (1 mmol), and ethyl acetoacetate (1 mmol) were stirred in 2 mL of ethanol in the presence of 30 mg of M-Ca 1 % at room temperature (20 °C) for 12 h

$CaCO_3$. After completion of the reaction, the recovered catalyst is washed with hot ethanol (2 × 3 mL) and dried in vacuum. The results, which are given in Table 4, suggest no appreciable variations when the catalyst is reused five consecutive times.

In order to evaluate the possible catalyst solubilization, an additional test was performed. The Ca-MCM 1 % sample (30 mg) was refluxed in ethanol (5 mL) for 12 h, filtered at high temperature and dried in vacuum till constant weight. The activity of the treated catalyst is practically the same as that of the fresh catalyst (97 % yields in 12 h). The refluxed ethanol was used as solvent for attempting the reaction without adding the catalyst. After 12 h of reaction, appreciable amounts of benzylidene-malononitrile intermediate, and Knoevenagel condensation product between benzaldehyde and ethyl acetoacetate, and only traces of product were detected.

The scope and generality of this procedure is illustrated by various examples using different aldehydes and methyl or ethylacetoacetate, and the results are summarized in Table 5. According to the results of optimization experiments for the reaction conditions, the reactions are carried out in the presence of catalyst (30 mg) at room temperature (20 °C) using ethanol as reaction solvent, and the corresponding 2-amino-4*H*-pyran derivatives are obtained in very good yields (Table 5, entries 1–7).

The workup and catalyst recovery are simple, and all reactions have very high selectivity toward the corresponding 2-amino-4*H*-pyran. The TLC analysis shows only trace amounts of by-products. After completion of the reaction (monitored by TLC, eluent; EtOAc:hexane mixtures), the catalyst was separated by centrifugation and washed with ethanol. After ethanol evaporation, the crude product was easily isolated in almost pure state. Further purification was performed by recrystallization from ethanol. The reaction solvent can be recovered by simple distillation and reused. The products are known compounds and were characterized by ^{1}H-NMR and ^{13}C-NMR spectroscopy. The characterization details of all compounds are shown in the experimental methods section.

A plausible reaction mechanism similar to that proposed by Das and coworkers using ZnO as catalyst can be considered [15]. We assume that our materials are bifunctional catalysts with acid sites provided by the MCM material surface and basic sites due to the presence of $CaCO_3$. As Fig. 8 shows, the reaction involves

Table 5 Synthesis of polyfunctionalized 2-amine-4*H*-pyran catalyzed by Ca-MCM 1 %

Entry	Ar	R	M. P.		Yield	
			Found	Lit.	Found	Lit.
1	C_6H_5	CH_3CH_2–	182–183	178–179 [21]	98	90
2	4–CH_3–C_6H_4	CH_3CH_2–	155–156	158 [15]	75	92
3	2–NO_2–C_6H_4	CH_3CH_2–	162–164	163–165 [21]	70	83
4	3–NO_2–C_6H_4	CH_3CH_2–	178–179	181 [33]	90	97
5	3–OH–C_6H_4	CH_3CH_2–	160–161	163–165 [33]	83	71
6	2–Cl–C_6H_4	CH_3CH_2–	179–180	179–181 [21]	77	91
7	3–OCH_3–C_6H_4	CH_3CH_2–	150–151	147–148 [34]	83	79
8	3,4,5–$(OCH_3)_3$–C_6H_2	CH_3CH_2–	183–184	181–183 [21]	58	88
9	4–OCH_3–C_6H_4	CH_3CH_2–	143–144	142–144 [35]	71	68
10	C_6H_5	CH_3–	157–159	160–162 [36]	98	96
11	4–CH_3–C_6H_4	CH_3–	162–163	164–165 [36]	73	93
12	2–Cl–C_6H_4	CH_3–	144–145	148–150 [36]	90	97

Reaction conditions Benzaldehyde (1 mmol), malononitrile (1 mmol), and ethyl acetoacetate (1 mmol) were stirred in 2 mL of ethanol in the presence of 30 mg of M-Ca 1 % at room temperature (20 °C) for 12 h

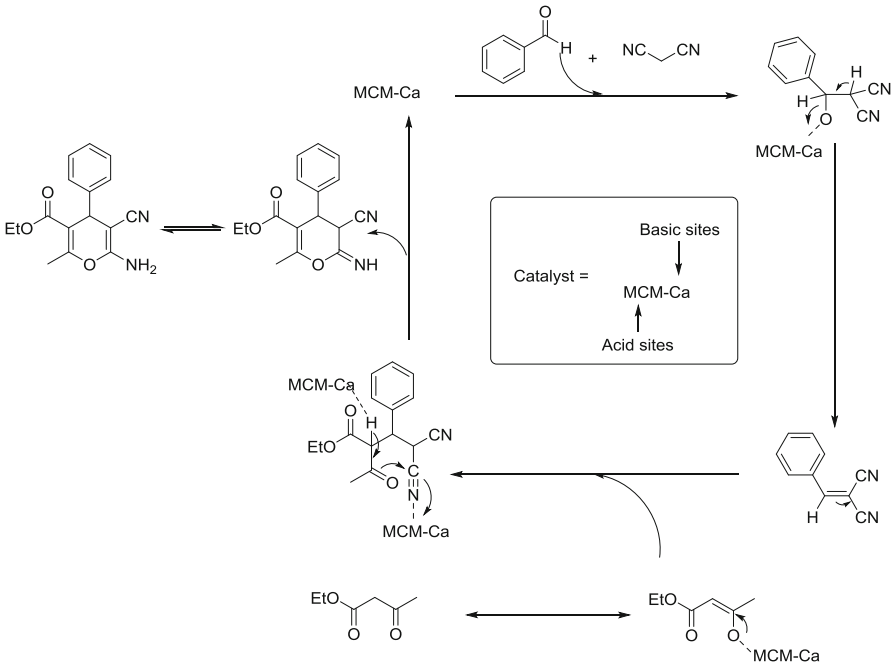

Fig. 8 Plausible mechanism for the synthesis of 4*H*-pyrans over Ca-MCM catalysts

successive Knoevenagel condensation, Michael addition, and finally intramolecular ring closure leading to the formation of 4*H*-pyran. In the first step, the Knoevenagel condensation between benzaldehyde and malononitrile was through bifunctional MCM-Ca, which removed the acidic proton from the methylene group present in the malononitrile acting as a base and in the dehydration acting as acid catalyst. In the ring closure, the catalyst acts as an acid, minimizing the repulsion between the germinal nitrile groups. Also, this activates one of the nitrile groups by polarization and facilitates the intramolecular nucleophilic attack by the enolic OH group, leading to the formation of the final product and catalyst regeneration.

Conclusion

In this paper, we report the synthesis and characterization of three mesoporous Ca-MCM catalysts with different calcium contents (1, 2, and 5 %), which were characterized by atomic absorption, XRD, FT-IR, XPS, TPD-CO_2, and textural properties (SBET). A green and simple protocol was developed for the synthesis of 6-amino-4*H*-pyran scaffolds through a multicomponent coupling reaction of an aldehyde, malononitrile, and 1,3-dicarbonyl compound in different reaction solvents. This procedure was performed at room temperature (20 °C), so good and excellent yields of 4*H*-pyran derivatives were obtained. The mesoporous materials are insoluble in polar media, which allows easy removal of the reaction products without affecting their catalytic activity. A series of substituted 4*H*-pyrans was synthesized using these materials and ethanol as solvent. This methodology requires a reaction time of approximately 12 h and room temperature (20 °C); using these conditions, excellent yields of 4*H*-pyran derivatives were obtained. The Ca-MCM catalysts are insoluble in polar media, which allows easy removal of the reaction products without affecting their catalytic activity. The applications of these catalysts in biomass valorization through multicomponent reactions are in progress in our laboratory.

Acknowledgments This work was supported by CONICET (PIP 003), ANPCyT (PICT 0409) and La Plata University. Also, the authors thank Colciencias for financial support under the project 110965843004. Contract: Colciencias-UPTC 047-2015. GPR and AGS are CONICET members. J. J. Martínez thanks CONICET-OEA for a short fellowship in the UNLP.

References

1. M. Bowker, Catal. Lett. **142**, 1411 (2012)
2. R.A. Sheldon, Chem. Soc. Rev. **41**, 1437 (2012)
3. J.M. Thomas, W.J. Thomas, *Principles and Practice of Heterogeneous Catalysis* (Wiley, London, 2014)
4. M.E. Pérez, D.M. Ruiz, M. Schneider, J.C. Autino, G. Romanelli, Cienc. Desarro. **4**, 83 (2013)
5. C. Capello, U. Fischer, K. Hungerbuhler, Green Chem. **9**, 927 (2007)
6. H. Hattori, Chem. Rev. **95**, 537 (1995)
7. H. Hattori, A. Satoh, J. Catal. **45**, 32 (1976)
8. K. Tanabe, W.F. Hölderich, Appl. Catal. A-Gen. **181**, 399 (1999)

9. J. Tantirungrotechai, P. Thananupappaisal, B. Yoosuk, N. Viriya-empikul, K. Faungnawakij, Catal Commun. **16**, 25 (2011)
10. Y. Kubota, Y. Nishizaki, H. Ikeya, M. Saeki, T. Hida, S. Kawazu, M. Yoshida, H. Fujii, Y. Sugi, Micropor. Mesopor. Mater. **70**, 135 (2004)
11. M. Pirouzmand, B. Nikzad-kojanag, S.K. Seyed-Rasulzade, Catal. Commun. **69**, 196 (2015)
12. J. Safaei-Ghomi, R. Teymuri, H. Shahbazi-Alavi, A. Ziarati, Chin. Chem Lett. **24**, 921 (2013)
13. G. Evano, N. Blanchard, M. Toumi, Chem. Rev. **108**, 3054 (2008)
14. A. Akbari, Z. Azami-Sardooei, A. Hosseini-Nia, J. Korean Chem. Soc. **57**, 455 (2013)
15. P. Bhattacharyya, K. Pradhan, S. Paul, A.R. Das, Tetrahedron Lett. **53**, 4687 (2012)
16. D. Armesto, W.M. Horspool, N. Martin, A. Ramos, C. Seoane, J. Org. Chem. **54**, 3069 (1989)
17. S. Banerjee, A. Horn, H. Khatri, G. Sereda, Tetrahedron Lett. **52**, 1878 (2011)
18. M.A. Nasseri, S.M. Sadeghzadeh, J. Iran. Chem. Soc. **10**, 1047 (2013)
19. M.G. Dekamin, M. Eslami, Green Chem. **16**, 4914 (2014)
20. M. Gupta, M. Gupta, V.K. Gupta, New J. Chem. **39**, 3578 (2015)
21. M.S. Pandharpatte, K.B. Mulani, N.N.G. Mohammed, J. Chin. Chem. Soc. **59**, 645 (2012)
22. M.M. Heravi, Y.S. Beheshtiha, Z. Pirnia, S. Sadjadi, M. Adibi, Synth. Commun. **39**, 3663 (2009)
23. A. Molla, E. Hossain, S. Hussain, RSC Adv. **3**, 21517 (2013)
24. H. Valizadeh, A.A. Azimi, J. Iran. Chem. Soc. **8**, 123 (2011)
25. F.M. Abdelrazek, M.H. Helal, A.S. Hebishy, S.M. Hassan, J. Heterocycl. Chem. **52**, 1026 (2015)
26. N. Seshu Babu, N. Pasha, K.T. Venkateswara Rao, P.S. Sai Prasad, N. Lingaiah, Tetrahedron Lett. **49**, 2730 (2008)
27. M.L. Deb, P.J. Bhuyan, Tetrahedron Lett. **46**, 6453 (2005)
28. B. Tian, X. Liu, C. Yu, F. Gao, S. Xie, B. Tu, D. Zhao, Chem. Commun. **11**, 1186 (2002)
29. H. Sun, J. Han, Y. Ding, W. Li, J. Duan, P. Chen, H. Lou, X. Zheng, Appl. Catal. A Gen. **390**, 26 (2010)
30. G. Eimer, S. Casuscelli, C. Chanquia, V. Elías, M. Crivello, E. Herrero, Catal. Today **133**, 639 (2008)
31. C. Otero-Areán, M. Rodríguez-Delgado, V. Montouillout, J.C. Lavalley, C. Fernandez, J.J. Cuart Pascual, J.B. Parra, Micropor. Mesopor. Mater. **67**, 259 (2004)
32. P.A. Jacobs, B.K.G. Theng, J.B. Uytterhoeven, J. Catal. **26**, 191 (1972)
33. F.K. Behbahani, F. Alipour, GU J. Sci. **28**, 387 (2015)
34. A. Moshtaghi Zonouz, I. Eskandari, D. Moghani, Chem. Sci. Trans. **1**, 91 (2012)
35. A. Sánchez, F. Hernández, P.C. Cruz, Y. Alcaraz, J. Tamariz, F. Delgado, M.A. Vázquez, J. Mex. Chem. Soc. **56**, 121 (2012)
36. R.M.N. Kalla, M.R. Kim, I. Kim, Tetrahedron Lett. **56**, 717 (2015)